II

Vibration Control

Nejat Olgac

11

Active Damping of Large Trusses

A. Preumont
Université Libre de Bruxelles

Frederic Bossens
Université Libre de Bruxelles

Nicolas Loix
Micromega Dynamics

Abstract

This chapter reviews various ways of damping large space trusses. The first part discusses the use of active struts consisting of a piezoelectric actuator collocated with a force sensor. The guaranteed stability properties of the integral force feedback are reviewed and the practical significance of the modal fraction of strain energy is stressed. The second part explains the concept of active tendon control of trusses; the similarity of this concept with the previous one is pointed out. The third part describes an active damping generic interface based on a Stewart platform architecture with piezoelectric legs. The similarity with the previous concepts is emphasized. Finally, the damping of microvibrations is briefly discussed.

11.1 Introduction

The development of future generations of ultralight and large space structures will probably not be possible without active damping enhancement of the structures and active isolation of the scientific payloads that are sensitive to vibrations. Interferometric missions are an example particularly stringent geometric stability requirements.[1,2] This chapter addresses the problem of active damping of large trusses with three different concepts: (i) active strut, (ii) active tendon, and (iii) generic interface. In all cases, the same control architecture is used: a collocated piezoelectric actuator and force sensor connected by a local controller with an integral force feedback (IFF).

11.2 Active Struts

The first concept is the most natural; it consists of replacing some passive bars in the truss by active struts (Figure 11.1). The active struts consist of a piezoelectric linear actuator (or another type of

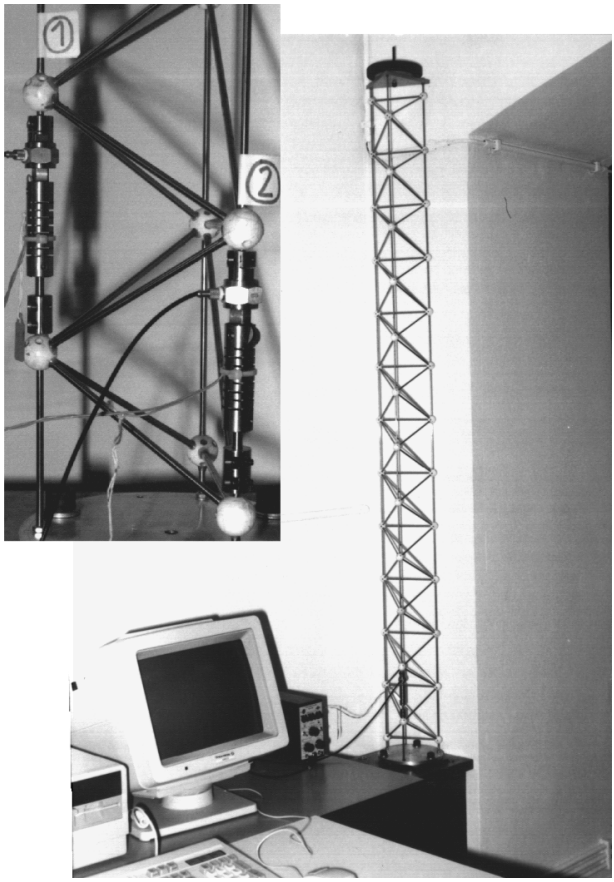

FIGURE 11.1 Active truss with piezoelectric struts (ULB).

linear displacement actuator such as magnetostrictive) co-linear with a force transducer. This concept was first demonstrated in the late 1980s.[3-6]

11.2.1 Open-Loop Dynamics of an Active Truss

Consider the active truss of Figure 11.2. when a voltage V is applied to an unconstrained linear piezoelectric actuator, it produces an expansion δ.

$$\delta = d_{33} n V = g_a V \tag{11.1}$$

where d_{33} is the piezoelectric coefficient, n is the number of piezoelectric ceramic elements in the actuator; g_a is the actuator gain. This equation neglects the hysteresis of the piezoelectric expansion. If the actuator is placed in a truss, its effect on the structure can be represented by equivalent piezoelectric loads acting on the passive structure. As for thermal loads, the pair of self-equilibrating piezoelectric loads applied axially to both ends of the active strut (Figure 11.2) has a magnitude equal to the product of the stiffness of the active strut, K_a, by the unconstrained piezoelectric expansion δ:

$$p = K_a \delta \tag{11.2}$$

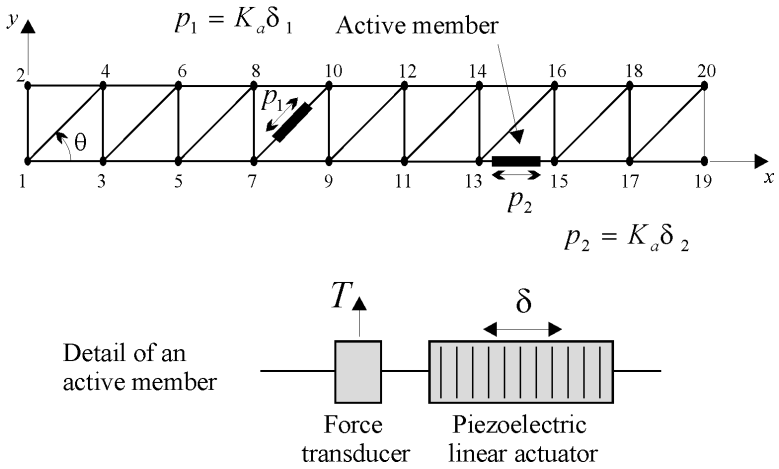

FIGURE 11.2 Active truss. The active struts consist of a piezoelectric linear actuator colinear with a force transducer.

Assuming no damping, the equation governing the motion of the structure excited by a single actuator is

$$M\ddot{x} + Kx = bp = bK_a\delta \tag{11.3}$$

where b is the influence vector of the active strut in the global coordinate system. The nonzero components of b are the direction cosines of the active bar. As for the output signal of the force transducer, it is given by

$$y = T = K_a\delta_e \tag{11.4}$$

where δ_e is the elastic extension of the active strut, equal to the difference between the total extension of the strut and its piezoelectric component δ. The total extension is the projection of the displacements of the end nodes on the active strut, $\Delta = b^T x$. Introducing this into Equation (11.4), we get

$$y = T = K_a(b^T x - \delta) \tag{11.5}$$

Note that because the sensor is located in the same strut as the actuator, the same influence vector b appears in the sensor Equation (11.5) and the equation of motion (11.3). If the force sensor is connected to a charge amplifier of gain g_s, the output voltage v_o is given by

$$v_0 = g_s T = g_s K_a(b^T x - \delta) \tag{11.6}$$

Note the presence of a feedthrough component from the piezoelectric extension δ. Upon transforming into modal coordinates, the frequency response function (FRF) $G(\omega)$ between the voltage V applied to the piezo and the output voltage of the charge amplifier can be written:[7]

$$\frac{v_0}{V} = G(\omega) = g_s g_a K_a \left\{ \sum_{i=1}^{n} \frac{\nu_i}{1 - \omega^2 / \Omega_i^2} - 1 \right\} \tag{11.7}$$

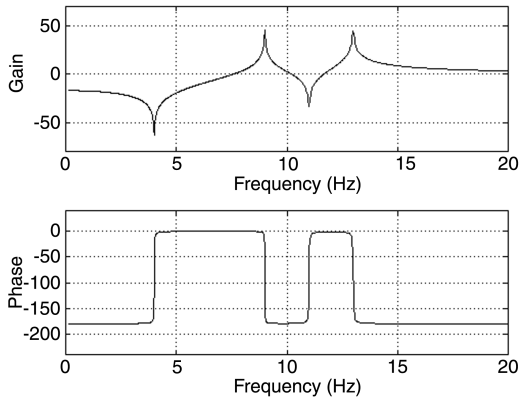

FIGURE 11.3 Open-loop FRF $G(\omega)$ of the active truss (a small damping is assumed).

where Ω_i are the natural frequencies, and we define

$$\nu_i = \frac{K_a(b^T\phi_i)^2}{\mu_i\Omega_i^2} = \frac{K_a(b^T\phi_i)^2}{\phi_i^T K\phi_i} \tag{11.8}$$

The numerator and the denominator of this expression represent, respectively, twice the strain energy in the active strut and twice the total strain energy when the structure vibrates according to mode i. $\nu_i(\geq 0)$ is, therefore, called the *modal fraction of strain energy* in the active strut. From Equation (11.7), we see that ν_i determines the residue of mode i, which is the amplitude of the contribution of mode i in the transfer function between the piezo actuator and the force sensor. It can, therefore, be regarded as a compound index of controllability and observability of mode i. ν_i is readily available from commercial finite element programs and can be used to select the proper location of the active strut in the structure: the best location is that with the highest ν_i for the modes that we wish to control.[5]

11.2.2 Integral Force Feedback

The FRF (Equation 11.7) has alternating poles and zeros (Figure 11.3) on the imaginary axis (or near if the structural damping is taken into account); on the other hand, $G(\omega)$ has a feedthrough component and some roll-off must be added to the compensator to achieve stability. It is readily established from the root locus (Figure 11.4) that the positive integral force feedback (IFF):

$$gD(s) = \frac{-g}{K_a s} \tag{11.9}$$

is unconditionally stable for all values of g. The negative sign in Equation (11.9) is combined with the negative sign in the feedback loop (Figure 11.5) to produce a positive feedback.

In practice, it is not advisable to implement plain integral control, because it would lead to saturation. A forgetting factor can be introduced by slightly moving the pole of the compensator from the origin to the negative real axis, leading to

$$gD(s) = \frac{-g}{K_a(s+\varepsilon)} \tag{11.10}$$

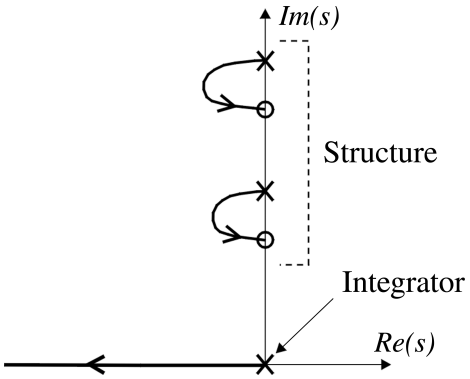

FIGURE 11.4 Root locus of the integral force feedback.

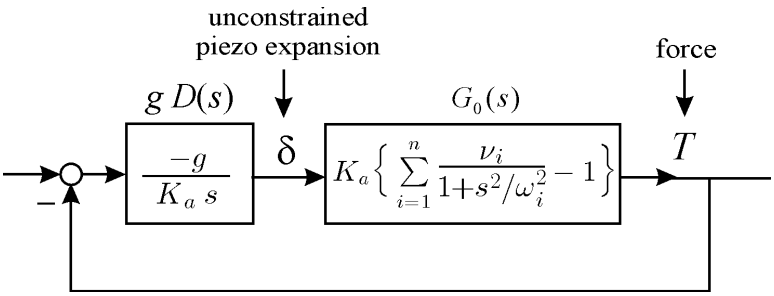

FIGURE 11.5 Block diagram of the integral force feedback.

This does not affect the general shape of the root locus and prevents saturation. Note that piezoelectric force sensors have a built-in high-pass filter.

11.2.3 Modal Damping

Combining the structure Equation (11.3), the sensor Equation (11.5), and the controller Equation (11.9), the closed-loop characteristic equation reads

$$\left[Ms^2 + K - \frac{g}{s+g}\left(bK_a b^T\right)\right]x = 0 \tag{11.11}$$

From this equation, we can deduce the open-loop transmission zeros, which coincide with the asymptotic values of the closed-loop poles as $g \to \infty$. Taking the limit, we get

$$\left[Ms^2 + (K - bK_a b^T)\right]x = 0 \tag{11.12}$$

which states that the zeros (i.e., the anti-resonance frequencies) coincide with the poles (resonance frequencies) of the structure where the active strut has been removed (corresponding to the stiffness matrix $K\text{-}bK_a b^T$).

To evaluate the modal damping, Equation (11.11) must be transformed in modal coordinates with the change of variables $x = \Phi z$. Assuming that the mode shapes have been normalized according to $\Phi^T M \Phi = I$ and taking into account that $\Phi^T K \Phi = diag(\Omega_i^2) = \Omega^2$, we have

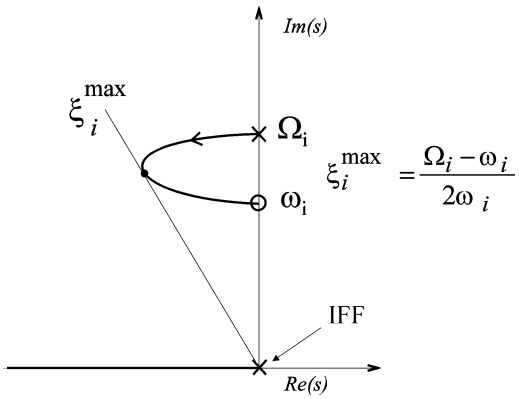

FIGURE 11.6 Root locus of the closed-loop pole for the IFF.

$$\left[Is^2 + \Omega^2 - \frac{g}{s+g} \Phi^T (bK_a b^T) \Phi \right] z = 0 \tag{11.13}$$

The matrix $\Phi^T(bK_a b^T)\Phi$ is, in general, fully populated. If we assume that it is diagonally dominant, and if we neglect the off-diagonal terms, it can be rewritten

$$\Phi^T (bK_a b^T) \Phi \approx \text{diag}(\nu_i \Omega_i^2) \tag{11.14}$$

where ν_i is the fraction of modal strain energy in the active member when the structure vibrates according to mode i; ν_i is defined by Equation (11.8). Substituting Equation (11.14) into Equation (11.13), we find a set of decoupled equations

$$s^2 + \Omega_i^2 - \frac{g}{s+g} \nu_i \Omega_i^2 = 0 \tag{11.15}$$

and, after introducing

$$\omega_i^2 = \Omega_i^2 (1 - \nu_i) \tag{11.16}$$

it can be rewritten

$$s^2 + \Omega_i^2 - \frac{g}{s+g} \left(\Omega_i^2 - \omega_i^2 \right) = 0 \tag{11.17}$$

By comparison with Equation (11.11), we see that the transmission zeros (the limit of the closed-loop poles as $g \to \infty$) are $\pm j\omega_i$. The characteristic equation can be rewritten

$$1 + g \frac{(s^2 + \omega_i^2)}{s(s^2 + \Omega_i^2)} = 0 \tag{11.18}$$

The corresponding root locus is shown in Figure 11.6. The depth of the loop in the left half plane depends on the frequency difference $\Omega_i - \omega_i$, and the maximum modal damping is given by

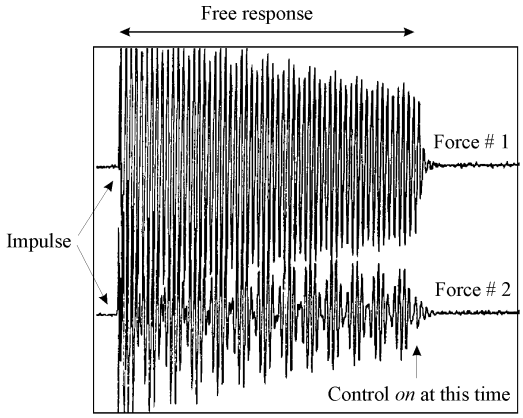

FIGURE 11.7 Force signal from the two active struts during the free response after impulsive load.

$$\xi_i^{\max} = \frac{\Omega_i - \omega_i}{2\omega_i} \tag{11.19}$$

It is obtained for $g = \Omega_i \sqrt{\Omega_i / \omega_i}$. For small gains, it can be shown that

$$\xi_i = \frac{g\nu_i}{2\Omega_i} \tag{11.20}$$

This interesting result tells us that, for small gains, the active damping ratio in a given mode is proportional to the fraction of modal strain energy in the active element. This result is very useful for the design of active trusses; the active struts should be located to maximize the fraction of modal strain energy ν_i in the active members for the critical vibration modes. The preceding results have been established for a single active member. If several active members are operating with the same control law and the same gain g, this result can be generalized under similar assumptions. It can be shown that each closed-loop pole follows a root locus governed by Equation (11.18) where the pole Ω_i is the natural frequency of the open-loop structure and the zero ω_i is the natural frequency of the structure where the active members have been removed.

11.2.4 Experimental Results

Figures 11.7 and 11.8 illustrate typical results obtained with the test structure of Figure 11.1. The modal damping ratio of the first two modes is larger than 10%. Note that in addition to being simple and robust, the control law can be implemented in an analog controller, which performs better in microvibrations.

11.3 Active Tendon Control

The use of cables to achieve lightweight spacecrafts is not new; it can be found in Herman Oberth's early books[17,18] on astronautics. In terms of weight, the use of guy cables is probably the most efficient way to stiffen a structure. They also can be used to prestress a deployable structure and eliminate the geometric uncertainty due to the gaps. One further step consists of providing the cables with active tendons to achieve active damping in the structure. This approach has been developed in References 7–12.

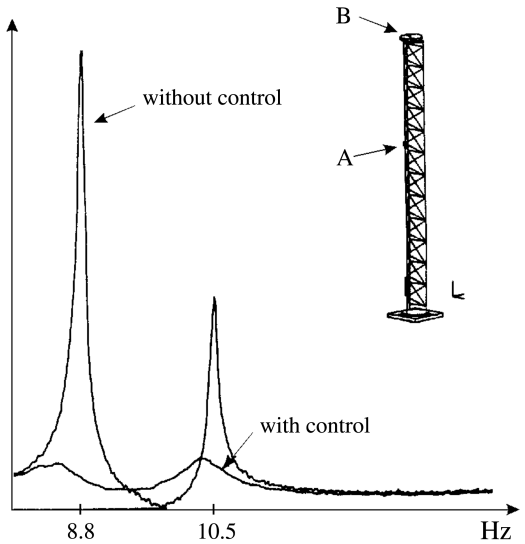

FIGURE 11.8 FRF between a force in A and an accelerometer in B, with and without control.

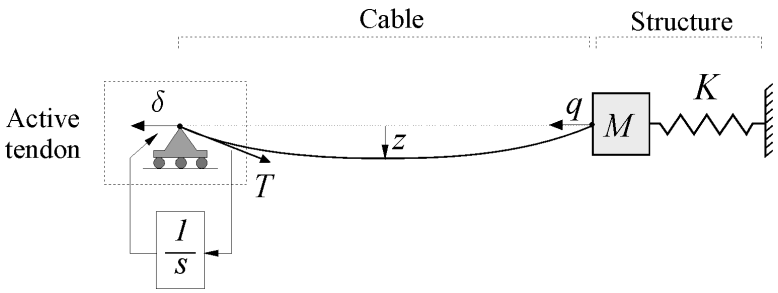

FIGURE 11.9 Active damping of cable structures.

11.3.1 Active Damping of Cable Structures

When using a displacement actuator and a force sensor, the (positive) integral force feedback Equation (11.9) belongs to the class of "energy absorbing" controls: indeed, if

$$\delta \sim \int T dt \tag{11.21}$$

the power flow from the control system is $W = -T\dot{\delta} \sim -T^2 \leq 0$. This means that the control can only extract energy from the system. This applies to nonlinear structures as well; all the states which are controllable and observable are asymptotically stable for all positive gains (infinite gain margin). The control concept is represented schematically in Figure 11.9 where the spring-mass system represents an arbitrary structure. Note that the damping introduced in the cables is usually very low, but experimental results have confirmed that it always remains stable, even at the parametric resonance, when the natural frequency of the structure is twice that of the cables. Whenever possible, however, the tension in the cables should be adjusted in such a way that their first natural frequency is above the frequency range where the global modes must be damped.

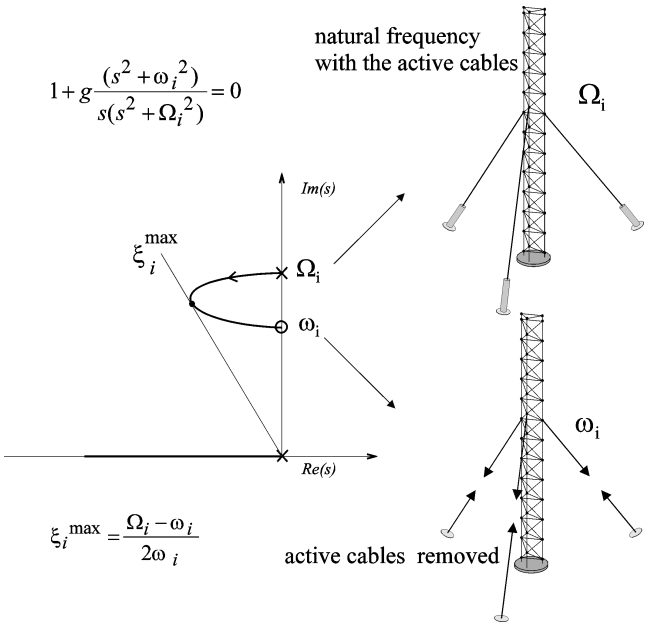

FIGURE 11.10 Root locus of the closed-loop poles.

11.3.2 Modal Damping

If we assume that the dynamics of the cables can be neglected and that their interaction with the structure is restricted to the tension in the cables, and that the global mode shapes are identical with and without the cables, one can develop an approximate linear theory for the closed-loop system. The following results that follow closely those obtained in the foregoing section (we assume no structural damping) can be established:

The open-loop poles are $\pm j\Omega_i$ where Ω_i are the natural frequencies of the structure including the active cables and the open-loop zeros are $\pm j\omega_i$ where ω_i are the natural frequencies of the structure where the active cables have been removed.

If the same control gain is used for every local control loop, as g goes from *0* to ∞, the closed-loop poles follow the root locus defined by Equation (11.18) and (Figure 11.10). Equations (11.19) and (11.20) also apply in this case.

11.3.3 Active Tendon Design

Figure 11.11 shows two possible designs of the active tendon: the first one (bottom left) is based on a linear piezoactuator from PI and a force sensor from B&K; a lever mechanism (top view) is used to transform the tension in the cable into a compression in the piezo stack, and amplifies the translational motion to achieve about 100 μm. This active element is identical to that in an active strut. In the second design (bottom center and right), the linear actuator is replaced by an amplified actuator from CEDRAT Research, also connected to a B&K force sensor and flexible tips. In addition to being more compact, this design does not require an amplification mechanism and tension of the flexible tips produces a compression in the piezo stack at the center of the elliptical structure.

11.3.4 Experimental Results

Figure 11.12 shows the test structure; it is representative of a scale model of the JPL-Micro-Precision-Interferometer[1] which consists of a large trihedral passive truss of about 9 m. The free-floating condition

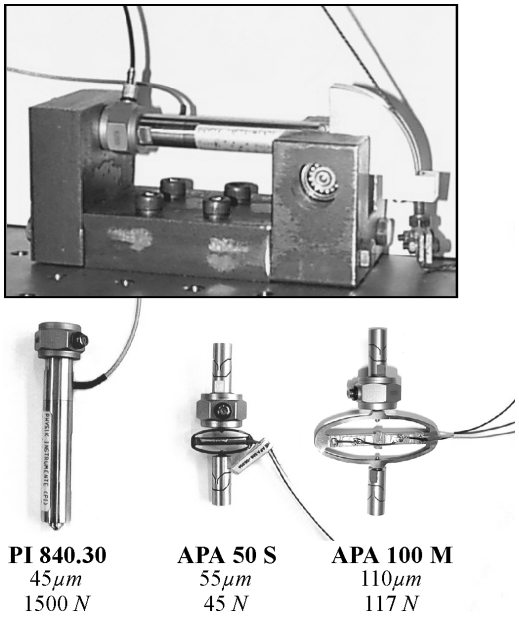

FIGURE 11.11 Three different designs of active tendon or active strut (ULB).

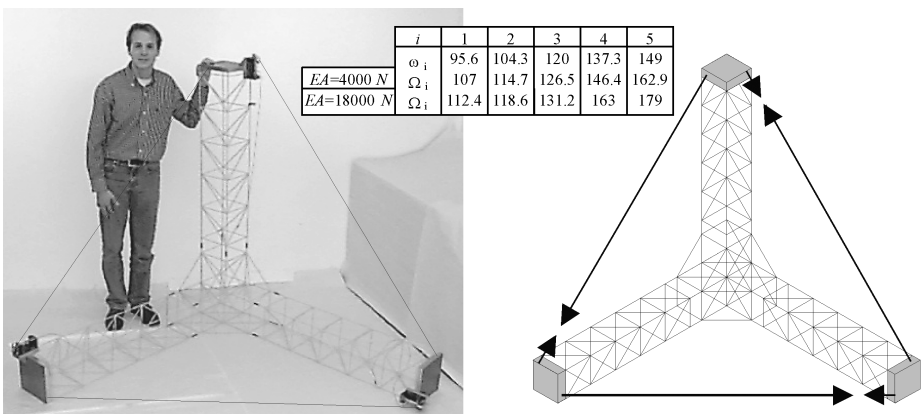

	i	1	2	3	4	5
	ω_i	95.6	104.3	120	137.3	149
EA=4000 *N*	Ω_i	107	114.7	126.5	146.4	162.9
EA=18000 *N*	Ω_i	112.4	118.6	131.2	163	179

FIGURE 11.12 Free floating truss with active tendons.

during the test is simulated by hanging the structure from the ceiling of the lab with soft springs. In this study, two different types of cables have been used: a fairly soft cable of 1-mm diameter of polyethylene ($EA \approx 4000N$) and a stiffer one of synthetic fiber *Dynema*™ ($EA \approx 18000N$). In both cases, the tension in the cables was chosen to set the first cable mode at 400 rad/sec or more, far above the first five flexible modes for which active damping is sought. The table inset in Figure 11.12 gives the measured natural frequencies ω_i (without cables) and Ω_i (with cables), for the two sets of cables.

Figure 11.13 compares the experimental closed-loop poles obtained for increasing gain g of the control with the root locus prediction of Equation (11.18). The results are consistent with the analytical predictions, although a larger scatter is observed with stiffer cables. Note, however, that the experimental results tend to exceed the root locus predictions. Figure 11.14 compares typical FRF with and without control. An analytical study was conducted[11] to investigate the possibility of using three Kevlar cables of *2* mm diameter connecting the tips of the three trusses of the JPL-MPI. Using

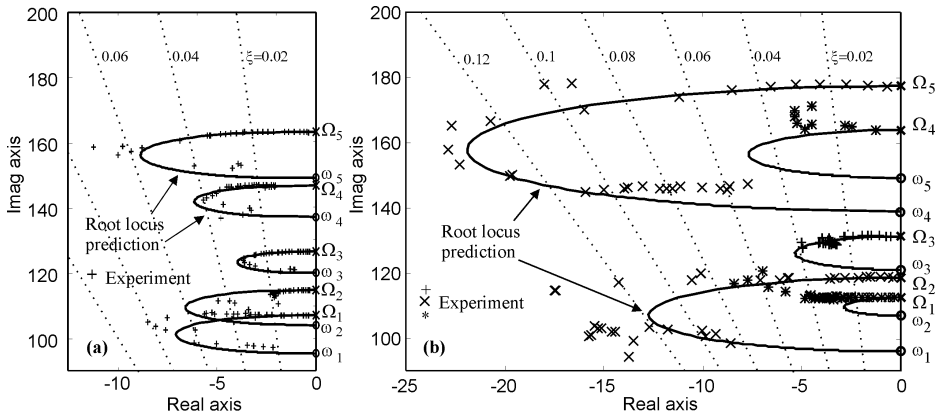

FIGURE 11.13 Experimental poles vs. root-locus prediction for the flexible modes of the free floating truss. (a) *EA = 4000 N*; (b) *EA = 18000 N*.

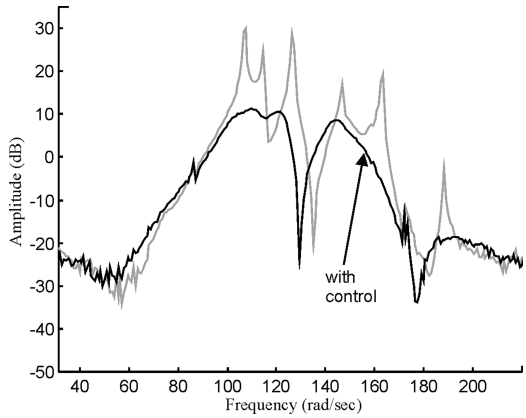

FIGURE 11.14 Typical FRF with and without control (*EA = 4000N*).

the root locus technique of Figure 11.10, a damping ratio between 14 and 21% was predicted in the first three flexible modes.

11.4 Active Damping Generic Interface

The active strut discussed in Section 11.2 can be developed into a generic six degrees-of-freedom interface which can be used to connect arbitrary substructures. Such an interface is shown in Figure 11.15; it consists of a Stewart platform with cubic architecture.[13] Each leg consists of an active strut similar to that shown at the center of Figure 11.11: a piezotranslator of the amplified design collocated with a force sensor, and connected to the base plates by flexible tips acting like spherical joints. The cubic architecture provides a uniform control capability in all directions, a uniform stiffness in all directions, and minimizes the cross-coupling among actuators (which are mutually orthogonal). The control is decentralized with the same gain for all loops. Figure 11.16 shows the generic interface mounted between a truss and the supporting structure. Figure 11.17 shows the evolution of the first two closed-loop poles when we increase the gain of the decentralized controller; the continuous line shows the root locus prediction of Equation (11.18); Ω_i are the open-loop natural frequencies, while ω_i are the high-gain asymptotes of the closed-loop poles. Figure 11.18 shows a typical FRF of the structure of Figure 11.16, with and without control of the Stewart platform.

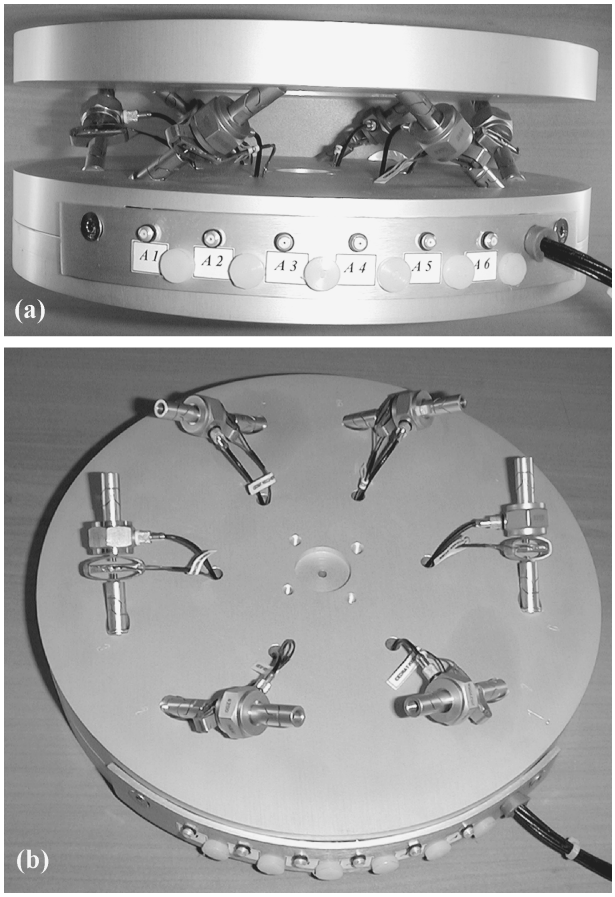

FIGURE 11.15 Stewart platform with piezoelectric legs as generic damping interface (a) general view; (b) the upper base plate removed.

11.5 Microvibrations

The performance and robustness of the control strategy have been experimentally demonstrated; however, most of the results presented in the literature have been obtained for vibration amplitudes in a range from millimeter to micron. For applications to precision space structures with optical payloads, it is essential that these results be confirmed for submicron vibrations,[14-16] despite the nonlinear behaviour of the actuator (hysteresis of the piezo).

It turns out that the performance limit of the control system is related to the sensitivity of the force sensor. This is illustrated in Figure 11.19, which shows the Lissajou plots δ vs. T (active tendon displacement vs. dynamic tension in the strut) for two sensors with different sensitivities. Because the control algorithm produces a 90° phase shift between the piezo extension and the force measurement, the theoretical shape of the plot is an ellipse; the area corresponds to the energy dissipation in the control system during one cycle. Figures 11.19 (a) and (c) on the left side have been obtained with a standard sensor (B&K 8200, 4 pc/N). The curve becomes more noisy as the vibration amplitude is reduced and the dynamic force approaches the sensitivity limit of the sensor. On the other hand, Figures 11.19 (b), (d), and (f), on the right side have been obtained with a more sensitive sensor (280000 pc/N). In this case, the Lissajou plots keep the right shape even for very small vibration amplitudes (the limit of this experiment actually came from background vibration).

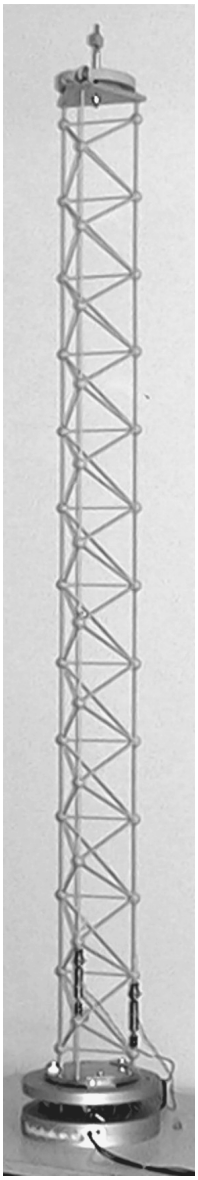

FIGURE 11.16 Generic active damping interface acting as a support of a truss.

11.6 Conclusions

This chapter reviewed various ways of damping large space trusses. The active strut consisting of a piezoelectric actuator collocated with a force sensor was described first. Next, three different ways to use this active strut to achieve active damping were reviewed: first by integrating the active strut as a member of the truss, next by using it as an active tendon in a cable structure, and finally by using the struts as the legs of a Stewart platform. The similarity between the various concepts has been pointed out when a decentralized controller is used, and it was shown that the closed-loop poles can be predicted with a root-locus technique. Finally, the damping of microvibrations was briefly discussed.

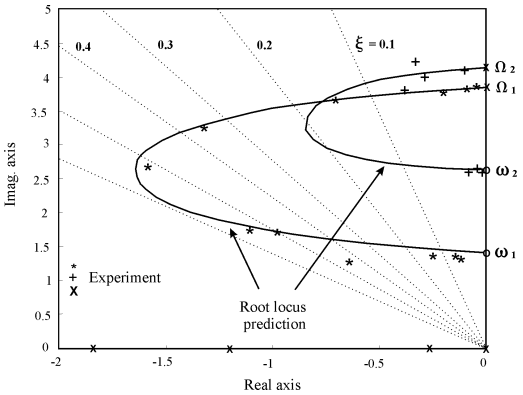

FIGURE 11.17 Experimental poles and root locus prediction from Equation (11.18).

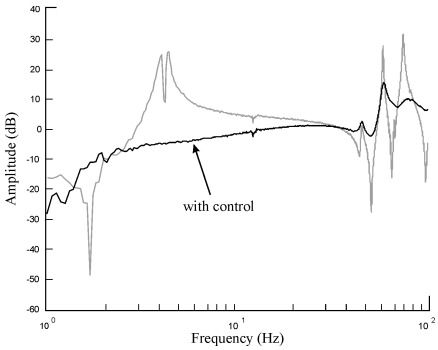

FIGURE 11.18 Typical FRF with and without control.

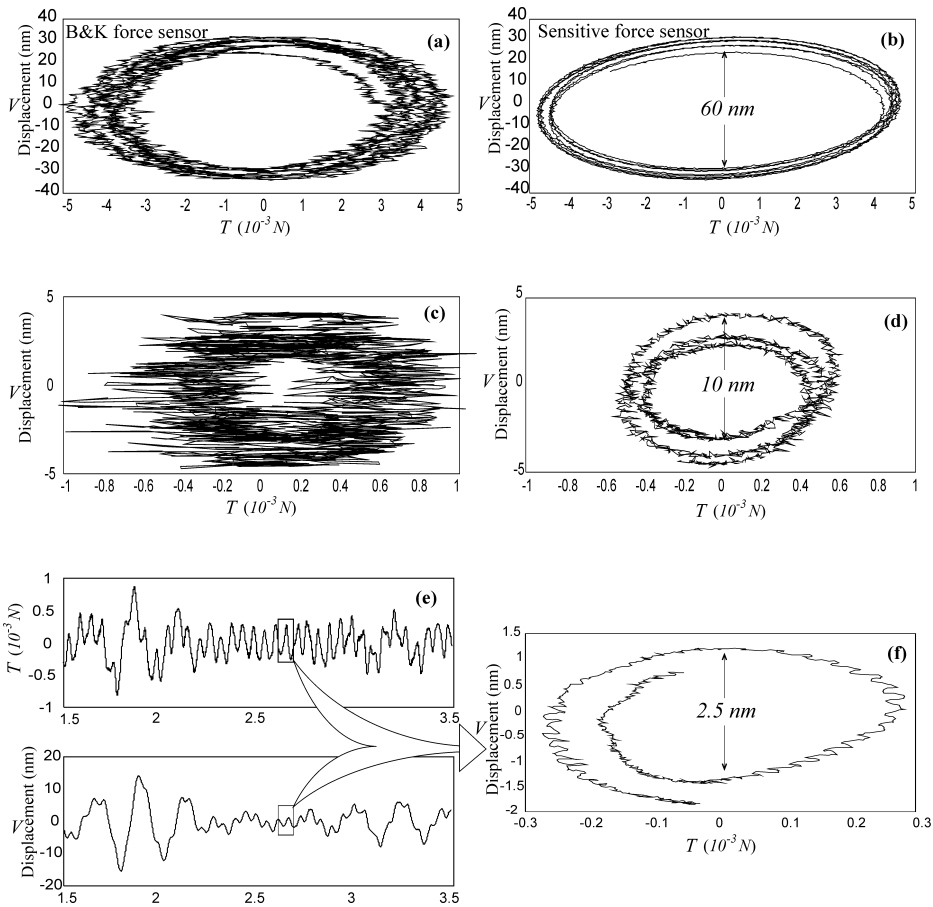

FIGURE 11.19 "Lissajou plots" δ vs. *T* in the microvibration range.

Acknowledgment

This study was partly supported by the Inter University Attraction Pole IUAP IV-24 on Intelligent Mechatronics Systems. The authors wish to thank Ahmed Abu Hanieh for his contribution to the design, manufacture, and testing of the Stewart platform.

References

1. Neat, G.W., Abramovici, A., Melody, J.M., Calvet, R.J., Nerheim, N.M., and O'Brien, J.F., Control technology readiness for spaceborne optical interferometer missions, *Proceedings SMACS-2,* Toulouse, 13–32 (1997).
2. Mallory, G.J.W., Saenz-Otero, A., and Miller, D.W., Origins test bed: Capturing the dynamics and control of future space-based telescopes, *Optical Engineering,* 39, 6, 1665–1676 (2000).
3. Fanson, J.L., Blackwood, C.H., and Chu, C.C., Active member control of a precision structure, *Proceedings of the 30th AIAA/ASME/ASCE/AHS Structures, Structural Dynamics, and Materials Conference,* AIAA, Washington, D.C., 1480–1494 (1989).
4. Chen, G.S., Lurie, B.J., and Wada, B.K., Experimental studies of adaptive structure for precision performance, *Proceedings of the 30th AIAA/ASME/ASCE/AHS Structures, Structural Dynamics, and Materials Conference,* AIAA, Washington, D.C.,1462–1472 (1989).
5. Preumont, A., Dufour, J.P., and Malekian, Ch., Active damping by a local force feedback with piezoelectric actuators, *AIAA, Journal of Guidance*, 15, 2, 390–395 (1992).
6. Peterson, L.D., Allen, J.J., Lauffer, J.P., and Miller, A.K., An experimental and analytical synthesis of controlled structure design, SDM Conference*,* AIAA paper 89-1170-CP (1989).
7. Preumont, A., *Vibration Control of Active Structures: An Introduction*, Kluwer Academic Publishers, Dordrecht (1997).
8. Achkire, Y., *Active Tendon Control of Cable-Stayed Bridges*, Ph.D. dissertation, Active Structures Laboratory, Université Libre de Bruxelles, Belgium, May 1997.
9. Achkire, Y. and Preumont, A., Active tendon control of cable-stayed bridges, *Earthquake Engineering and Structural Dynamics*, 25, 6, 585–597, June 1996.
10. Preumont, A. and Achkire, Y., Active damping of structures with guy cables, *AIAA, Journal of Guidance, Control, and Dynamics*, 20, 2, 320–326, March-April 1997.
11. Preumont, A., Achkire, Y., and Bossens, F., Active tendon control of large trusses, *AIAA Journal*, 38, 3, 493–498, March 2000.
12. Preumont, A. and Bossens, F., Active tendon control of vibration of truss structures: Theory and experiments, *Journal of Intelligent Material Systems and Structures,* 11, 2, 91–99, 2000.
13. Geng, Z.J. and Haynes, L.S., Six degrees-of-freedom active vibration control using the Stewart platforms, *IEEE Transactions on Control Systems Technology*, 2, 1, 45–53, 1994.
14. Peterson, L.D., Lake, M.S., and Hardaway, L.M.R., Micron accuracy deployment experiments (MADE): A space station laboratory for actively controlled precision deployable structures technology, *Proceedings of the Space Technology and Applications International Forum*, Albuquerque (NM), February 1999.
15. Ingham, M.D. and Crawley, E. F., Microdynamic characterization of modal parameters for deployable space structure, *AIAA Journal*, 39, 2, 331–338, February 2001.
16. Hardaway, L.M.R. and Peterson, L.D., Microdynamics of a precision deployable optical truss, *SPIE Paper No. 3785-01, Proceedings of the SPIE Annual Meeting*, Denver (Colorado), July 1999.
17. Oberth, H., *Man into Space*. *New Projects for Rocket and Space Travel* (translated from German by G.P.H. DeFreville), Weidenfeld and Nicolson, London, 1957.
18. Walters, H.B., *Hermann Oberth: Father of Space Travel*, Macmillan, New York, 1962.